

Supplement of *Clim. Past*, 13, 421–436, 2017  
<http://www.clim-past.net/13/421/2017/>  
doi:10.5194/cp-13-421-2017-supplement  
© Author(s) 2017. CC Attribution 3.0 License.



*Supplement of*

## **Reconstructing paleoclimate fields using online data assimilation with a linear inverse model**

**Walter A. Perkins and Gregory J. Hakim**

*Correspondence to:* Walter A. Perkins (wperkins@uw.edu)

The copyright of individual parts of the supplement might differ from the CC-BY 3.0 licence.

## **S1 Computational Expense**

On our desktop workstation (4-core CPU @ 3.4 GHz), the time required for a single iteration for a 151-year reconstruction with 100 ensemble members and using 110 proxies is between 1.5 – 2 minutes. Thus, a full experiment with 1200 100-member reconstructions (100 iterations for each of the 12 blending coefficients), takes around 40 hours. However, the iterations themselves can be run in parallel on different nodes of a computing cluster. In comparison, the offline method (no forecasting) takes about 1 minute to complete a single iteration. Therefore, the addition of the LIM approximately doubles the computational expense in the worst case, but the total wall-clock time is still quite manageable for large experiments. We have not taken steps to fully optimize the code so there are likely ways to lower the overall computational expense.

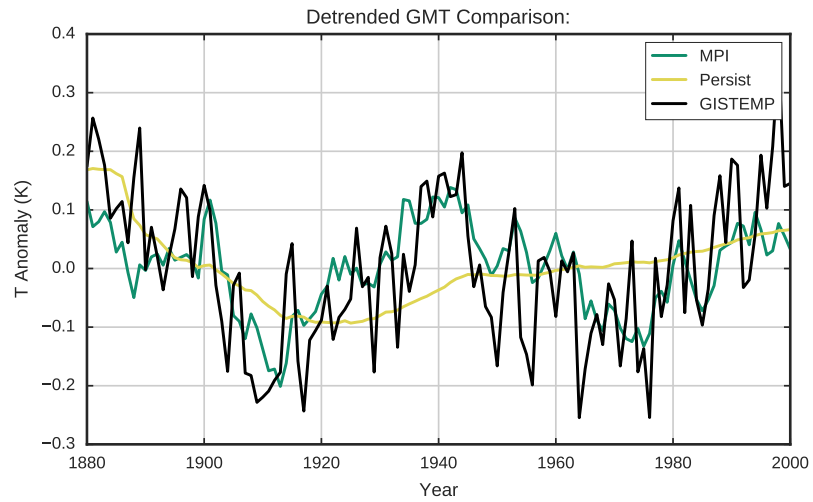


**Figure S1.** Reconstructed global mean 2m air temperature compared to GISTEMP (solid black) for the MPI LIM ( $a = 0.95$ ) and the persistence ( $a = 1.0$ ) experiment. The MPI case was chosen for comparison because it achieved a similar CRPS as the persistence case for a high blending coefficient.

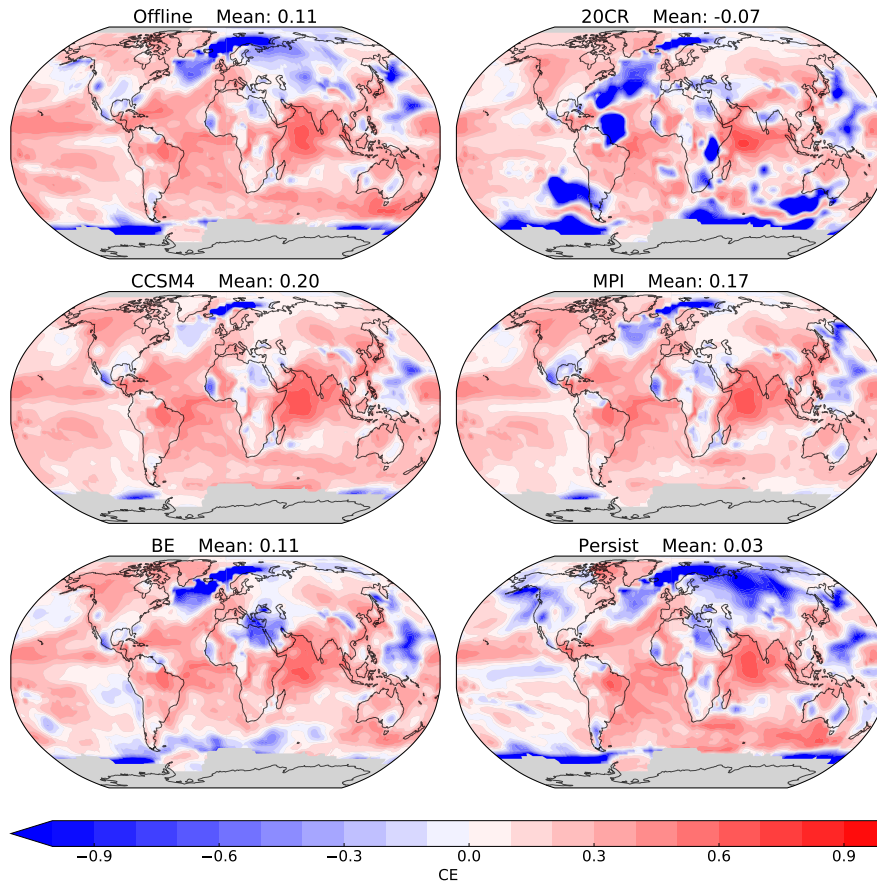


**Figure S2.** Spatial CE map. Each forecasting experiment shown uses the blending coefficient that achieves the highest full GMT CE skill (CCSM4:  $a = 0.9$ , MPI:  $a = 0.9$ , 20CR:  $a = 0.9$ , BE:  $a = 0.7$ ) except for the persistence case where  $a = 0.9$  was used. The area-weighted global mean for each experiment is shown in the title.

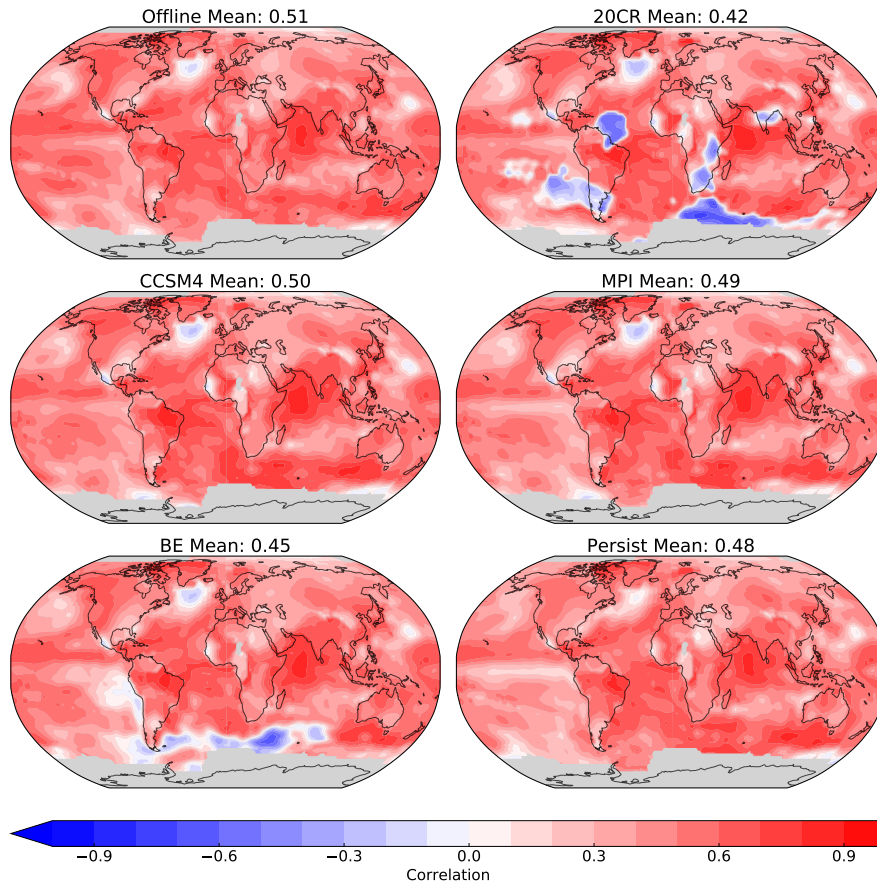


**Figure S3.** Spatial correlation map. Each forecasting experiment shown uses the blending coefficient that achieves the highest full GMT CE skill (CCSM4:  $a = 0.9$ , MPI:  $a = 0.9$ , 20CR:  $a = 0.9$ , BE:  $a = 0.7$ ) except for the persistence case where  $a = 0.9$  was used. The area-weighted global mean for each experiment is shown in the title.

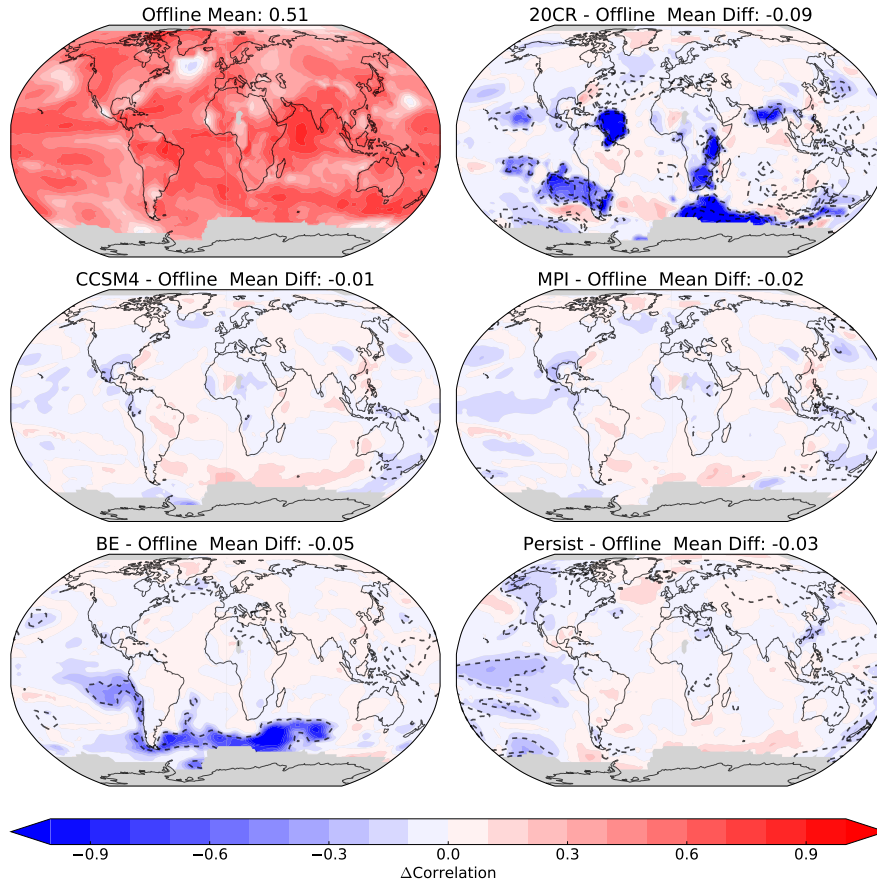


**Figure S4.** Spatial maps displaying the difference in correlation from the offline case. Difference maps are displayed for each forecasting experiment using the blending coefficient that achieves the highest full GMT CE skill (CCSM4:  $a = 0.9$ , MPI:  $a = 0.9$ , 20CR:  $a = 0.9$ , BE:  $a = 0.7$ ) except for the persistence case where  $a = 0.9$  was used. As a convenience contours of CE decreases are overlaid for each experiment in order to illustrate CE decreases associated with changes to correlation. The three contours shown are for CE changes of -0.25, -1.0, and -2.0. All global mean correlation differences are significantly different than the offline case with 95% confidence.

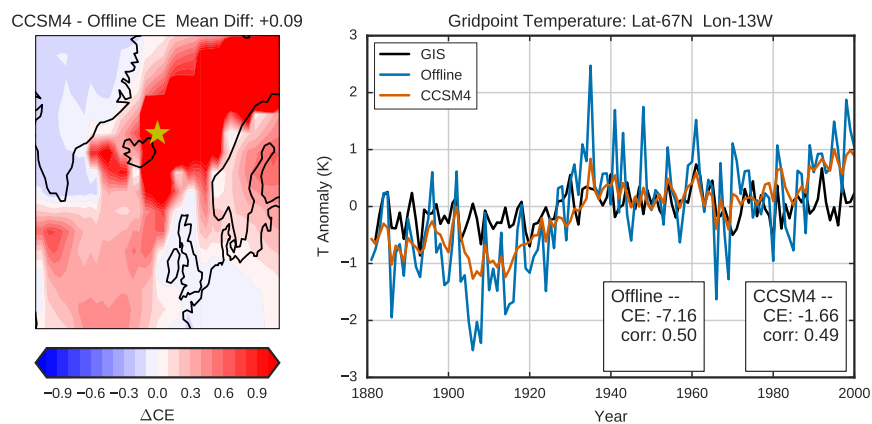


**Figure S5.** (Left) Spatial CE changes between the CCSM4 LIM ( $\alpha = 0.9$ ) and offline experiments in the North Atlantic/Barents Sea region. (Right) Grid point (located at the starred point on the left) 2m air temperature time series comparison between GISTEMP, the CCSM4 LIM reconstruction, and offline values.

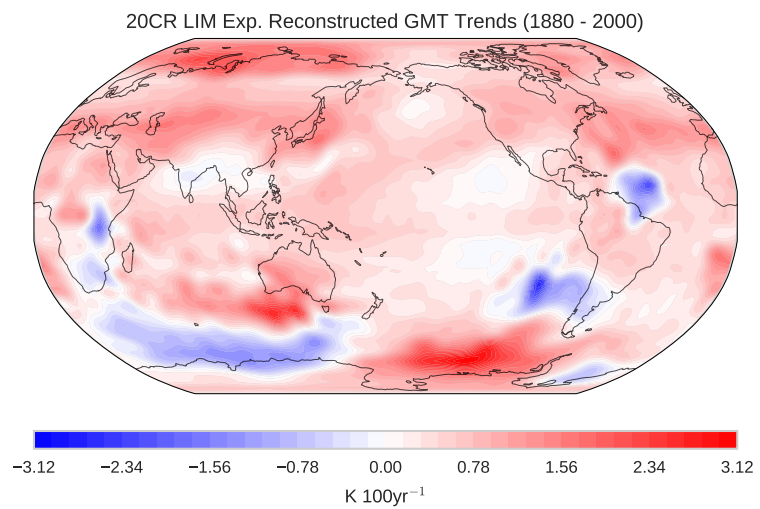


**Figure S6.** Spatial map of reconstructed 2m air temperature trends (1880–2000) for the 20CR LIM experiment at the blending coefficient  $a = 0.9$ .